Zigzag domains caused by strain-induced anisotropy of the Dzyaloshinskii-Moriya interaction

M. V. Sapozhnikov [1,2] R. V. Gorev,[1] E. V. Skorokhodov,[1] N. S. Gusev,[1] A. V. Sadovnikov [3] and O. G. Udalov[1,2,4]

[1]*Institute for Physics of Microstructures RAS, Nizhny Novgorod, 603950, Russia*
[2]*Lobachevsky State University of Nizhny Novgorod, 603950 Nizhny Novgorod, Russia*
[3]*Saratov State University, Saratov, 410012, Russia*
[4]*Department of Physics and Astronomy, California State University Northridge, Northridge, California 91330, USA*

The influence of the anisotropic interfacial Dzyaloshinskii-Moriya interaction (iDMI) on the structure of magnetic domains in thin Co/Pt films is investigated using magnetic force microscopy. The iDMI anisotropy is induced via application of strong (0.08%) in-plane uniaxial mechanical strain. We observe transformation of an isotropic labyrinth domain structure to oriented stripe domains and zigzag domain structures. According to theoretical considerations, such a transformation appears due to strain-induced strong iDMI anisotropy and change of iDMI sign along the direction perpendicular to the deformation axis.

I. INTRODUCTION

Magnetic domains were discovered 80 years ago [1]. Later, Landau and Lifshitz [2] explained the structure of domains and domain walls (DWs) taking into account exchange coupling, magnetocrystalline anisotropy, and magnetostatic interaction. At the present moment, DWs in ferromagnetic thin film are still intensively studied both experimentally [3–9] and theoretically [10–14]. The reason for this is that DWs are considered promising information carriers in racetrack devices for data storage [15], transfer [16], and processing [17].

Creating such devices requires an effective way to manipulate DWs in magnetic films. Local tuning of material parameters with irradiation was utilized to create domain structures with arbitrary topology [24,25]. This method, however, cannot be used for dynamical manipulation of DWs. A few approaches based on electric current were used to move domain walls [4,10]. Nevertheless, manipulating DWs with electric field is considered as a more attractive alternative due to low heat dissipation. Various magnetoelectric effects were used previously to tune thin-film magnetic structures [18–21]. Either exchange coupling [22] or magnetic anisotropy were varied in magnetic films [23] via application of an electric field.

The Dzyaloshinskii-Moriya interaction (DMI) [26–28] also affects the domain structure. This interaction becomes especially important in thin multilayer films with heavy metal (Pt,Ir,W)–ferromagnet (Fe, Co) interfaces [27–29]. In such systems, it is called the interfacial DMI (iDMI). A strong enough iDMI leads to formation of the Neel DWs [28]. This had been experimentally verified by spin-polarized low-energy electron microscopy [30] and the Lorentz transmission electron microscopy [31]. The micromagnetic problem of the domain width and DW structure in the film with the iDMI was solved in [32]. It was found that the competition between the iDMI and magnetostatic energies caused a fluent transition from the Bloch wall to the Neel one via a canted wall state.

Recently, it was demonstrated that the iDMI can be controlled with a mechanical strain [33,34]. The magnitude and the anisotropy of the iDMI can be tuned in a wide range this way. Interestingly, even the sign of the iDMI can be changed using mechanical deformations. Micromagnetic simulations and analysis [35] showed that skyrmions, antiskyrmions, and bimerons can be controlled if one can tune the iDMI anisotropy in a thin magnetic film. Taking into account that the strain can be induced with an electric field in the hybrid ferroelectric-ferromagnetic systems [36,37], this creates an additional mean to control magnetic topological structures and domain walls in magnetic films with the electric field.

Another recent calculation [38] predicted that the iDMI anisotropy should lead to essential magnetic domain structure transformation. In particular, the formation of the zigzag-shaped domain structures can take place.

These recent simulations and experimental findings stimulate the present work where we use strain to induce the iDMI anisotropy and experimentally study the magnetic domain structure of thin magnetic Co/Pt multilayer films with perpendicular magnetic anisotropy. The schematic of our experiment and main findings are shown in Fig. 1. We observe that the domain structure symmetry follows the symmetry of iDMI [measured by the Brillouin light scattering (BLS)] which is in agreement with the theoretical predictions made in Ref. [38]. Our findings confirm the ability to control magnetic film structure via strain-dependent iDMI.

II. SAMPLES AND METHODS

The magnetic multilayer films consisting of alternating layers of Co (0.7 nm) and Pt (1.1 nm, four periods) are deposited by magnetron sputtering in an Ar atmosphere (pressure 0.5 P)
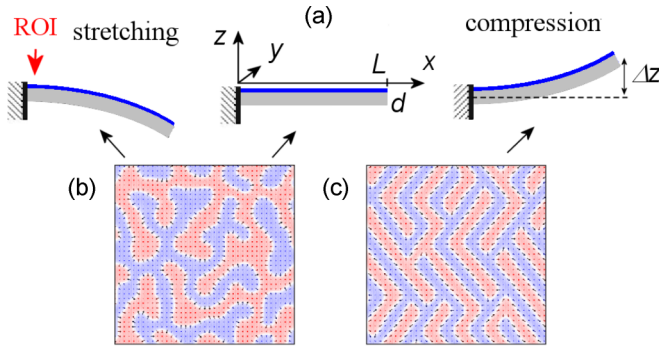
FIG. 1. (a) Geometry of the measurements. Values L and d are the sample length and thickness (including a substrate). The gray part of the sample is the substrate and the blue part is a multilayer magnetic film. One end of the sample is fixed, while the other one can be bent inducing a mechanical strain in the magnetic film. The shift Δz defines the strain magnitude. The red arrow shows the region of interest (ROI) with the highest deformation. All the measurements (MFM, MOKE, BLS) are performed in this region. (b) The schematic representation of an isotropic labyrinth domain structure observed in the undeformed sample. (c) Zigzag domains observed in the compressed film.

FIG. 2. (a) The typical MOKE hysteresis loop of the sample. ϕ is the rotation angle of a light polarization plane. H_s is the saturation field; H_d is the demagnetizing onset field. (b) Typical Stokes component of the BLS spectrum (scattered intensity as a function of frequency) for our samples. The red squares show the BLS intensity for the external magnetic field $H = 1$ T. The blue circles correspond to the external magnetic field $H = -1$ T. Solid lines are Lorentzian fits. Δf is the frequency shift cause by the iDMI.

on a glass plate (200-μm thickness) with Ta (10 nm)/Pt (10 nm) buffer sublayers. The growth rate is 0.25 nm/s for Pt and 0.125 nm/s for Co. The Pt top layer is 3 nm to protect the structure from oxidation. The accuracy of the deposition of layers in thickness is $\sim$10%.

We use magnetic force microscopy (MFM) to visualize magnetic domain structures at zero external magnetic field. A sample is fixed in a specially designed holder [see Fig. 1(a)]. While one edge of the sample is fixed, the opposite edge can be bent by a screw inducing uniaxial strain in the vicinity of the fixed side. Note that the strain appears along the sample long side (x axis) and no strain appears along the y axis. So, the in-plane strain is anisotropic. The x component of the strain can be estimated as $\varepsilon_{xx} = 3d\Delta z/4L^2$ [39], where d and L (typically $12 \div 16$ mm) are the thickness and length of the sample (glass plate), respectively, and Δz is the shift of the plate's free end ($0 \div 1$ mm). The out-of-plane strain is nonzero as well and defined by the Poisson ratio of the film. The holder allows us to carry out MFM measurements of the samples under application of the uniaxial strain. A phase shift of the probe oscillations is registered as an MFM signal. The MFM measurements are performed using both the two-pass tapping mode and the noncontact constant-height mode. Prior to the measurements, the MFM probes are magnetized along the tip axis in a 1-T external magnetic field. The sample and tip are grounded to avoid electrostatic effects [40]. The scan size is 10×10 μm^2 (512×512 pixels) to obtain appropriate power Fourier transformation diagrams. Prior to each measurement, the sample is demagnetized in a decaying alternating perpendicular external field. This procedure guarantees that the area of the domains with opposite magnetization would be equal. The measurements are performed for the range of applied strain $\varepsilon_{xx} = \pm 0.08\%$ with the step of 0.02%.

Magnetization hysteresis loops [see typical loop in Fig. 2(a)] are obtained by the magneto-optic Kerr effect

(MOKE) measurements in polar geometry and in a field up to 300 mT. A stabilized He-Ne ($\lambda = 632$ nm, 5 mW power) laser is used as a light source. Multiple samples were examined using MOKE to select those in which perpendicular anisotropy is combined with weak pinning of the domain walls. Such a combination can appear when the domain wall energy is low. In such samples, the field of the demagnetization onset (H_d) is close in magnitude to the saturation field (H_s). The samples having smaller $\Delta H_{sd} = H_s - H_d$ are more sensitive to iDMI variations and have smaller domains, which is more convenient for MFM measurements and further statistical analysis.

The iDMI is measured using the Brillouin light scattering (BLS) in the Damon-Eshbach geometry [41]. The similar holder as described above is used to apply the strain to the samples during the BLS measurements. To measure the iDMI constants along the x (D_x) and y (D_y) directions we turn the deformed sample by 90° around the out-of-plane axis. A typical BLS spectrum is presented in Fig. 2(b). Solid lines show the Lorentzian fit, demonstrating the shift (Δf) of the Stokes and anti-Stokes peaks. Following the standard approach, we estimate the iDMI constant as [41]

$$D_{x,y} = 2M_s\Delta f/(\pi\gamma k_{x,y}). \quad (1)$$

Here M_s is the saturation magnetization, $\gamma = 176$ GHz/T is the gyromagnetic ratio, and $k_{x,y}$ is the wave vector along the x or y direction. When we perform the iDMI constant calculations we consider the multilayer film as a homogeneous medium with some effective parameters. This is reasonable since the Pt thickness is small and there is a strong exchange interaction between Co layers [42]. So, all magnetic layers should have a joint domain structure. The value of M_s used for our estimates is 2.3×10^5 A/m. This value looks underestimated comparing to the value of the bulk Co magnetization. This is because the Co layers are interleaved with the Pt layers reducing the effective magnetization of the whole film. Previous experimental studies show that such a low effective magnetization describes properties of multilayer Co/Pt structures well [43–45]. Note that the iDMI coefficients calculated
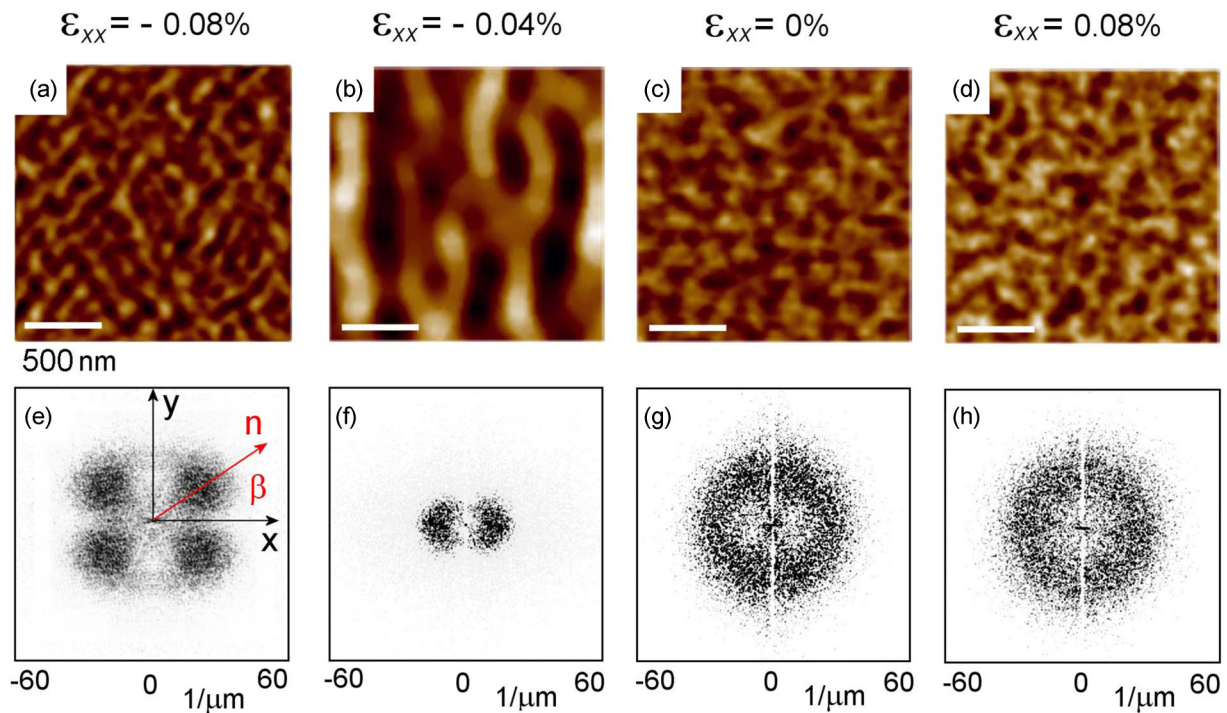
FIG. 3. (a)–(d) (Upper row) MFM images of domain structures for different applied strain (ε_{xx}). (a) $\varepsilon_{xx} = -0.08\%$, (b) $\varepsilon_{xx} = -0.04\%$, (c) $\varepsilon_{xx} = 0$, (d) $\varepsilon_{xx} = 0.08\%$. (Bottom line) (e)–(h) Spatial Fourier transforms of the domain structures. White color corresponds to the Fourier harmonic with zero amplitude. Black color corresponds to the Fourier harmonics with high amplitude. Strain is applied along the x axis. β is the average angle between the DWs orientation (**n**) and the strain direction. The vertical white line in the center of the diagrams is an artefact of image processing.

in Eq. (1) are also the effective characteristics of the whole film and not the iDMI coefficient for a single Co/Pt interface. The value of the perpendicular anisotropy can be estimated using the BLS measurements (Supplemental Material [33]) and is $K \sim 4 \times 10^4$ J/m^3. This value is in good agreement with the data of previous studies of similar Co/Pt multilayer films [43,45].

As it was shown in Ref. [46] the difference in the surface anisotropy of a magnetic film at the interfaces with a vacuum and a heavy metal can lead to the appearance of nonreciprocity in the propagation of spin waves, similar to the one produced by DMI. For typical anisotropy difference value of ~ 1 mJ/m^2, this contribution to the nonreciprocity exceeds the DMI contribution at thickness larger than $15 \sim 20$ nm. In films with several nanometers thickness (as we have), the non-reciprocity associated with the DMI is several times or even an order of magnitude greater than the nonreciprocity associated with the difference in anisotropy [47]. In our multilayer films, the surface anisotropy value also varies from layer to layer, but this variation can be estimated as $\sim 4 \times 10^{-2}$ mJ/m^2 [48] which is much lower than ~ 1 mJ/m^2. Therefore, we can safely assume that the observed nonreciprocity of spin waves in our BLS measurements is due to the DMI.

III. EXPERIMENTAL RESULTS AND DISCUSSION

The results of the MFM studies are presented in Fig. 3. The upper row shows typical domain structures of our sample. The undeformed sample [Fig. 3(c)] has a labyrinth domain structure with an isotropic orientation of domain walls. The

magnetic structure does not experience noticeable changes when the tensile strain up to $\varepsilon_{xx} = 0.08\%$ is applied to the sample [see Fig. 3(d)]. The situation is different when the sample is compressed. Stripe domains occur with a compressive strain of $\varepsilon_{xx} = -0.04\%$ [see Fig. 3(b)]. At that, the domains are oriented perpendicular to the deformation axis. Further compression [$\varepsilon_{xx} = -0.06\%, -0.08\%$; see Fig. 3(a)] leads to formation of domains oriented by the angle β with respect to the strain direction. Note that there are four equivalent DW orientations ($\pm\beta$ and $\pi \pm \beta$). Here and below, β is the angle between the normal vector (**n**) to a DW plane and the deformation direction (x axis).

For a quantitative analysis of the domain structures, a spatial Fourier transform of the MFM images is performed. The corresponding spatial Fourier spectra are shown in the bottom row in Fig. 3. For better visibility the images of the central part of the Fourier spectra are presented, since there are no short-wavelength harmonics in the MFM images of the domains. In the case of an undeformed and stretched samples [Figs. 3(g) and 3(h)], the Fourier diagram has the form of a ring, which corresponds to an isotropic labyrinth domain structure. The vertical white stripe observed in the diagrams is an artefact caused by the image processing procedure. The Fourier spectrum of the compressed sample [$\varepsilon_{xx} = -0.04\%$; Fig. 3(f)] shows two maxima, which correspond to formation of the stripe domains with $\beta = 0$. Further compression ($\varepsilon_{xx} = -0.06\%$ and -0.08%) leads to the appearance of 4 maxima. This means that the DWs prefer to orient along one of four equivalent directions at a certain angle β with respect to the strain axis and the zigzag domain structure appears.
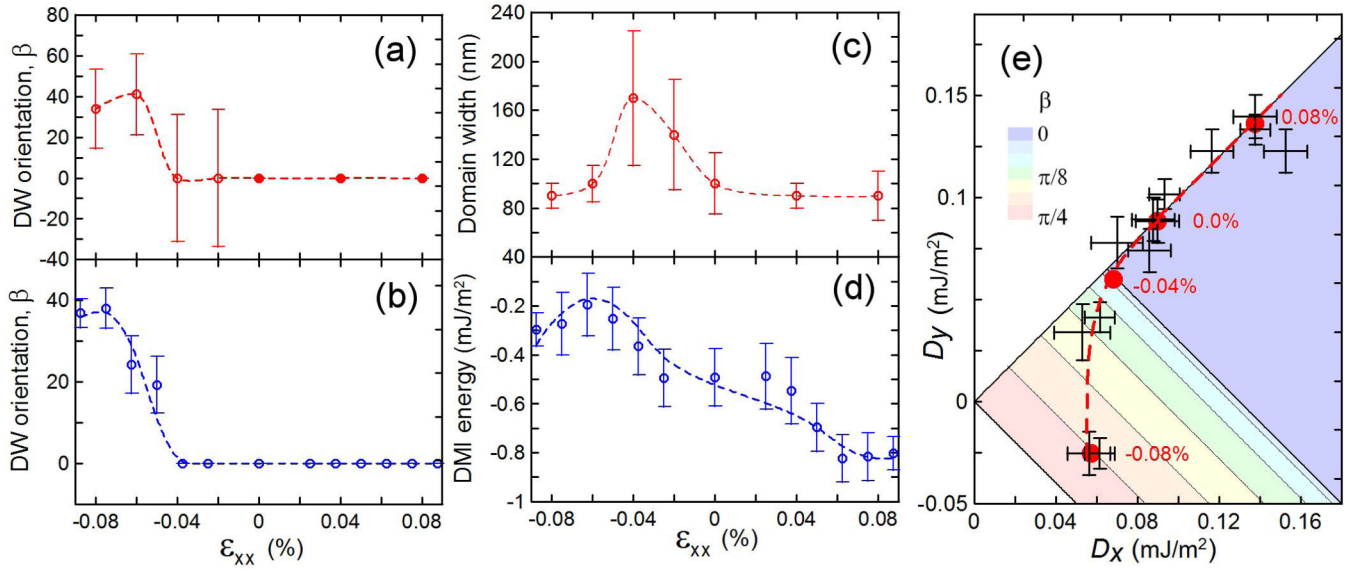
FIG. 4. (a) Average angle of the DW orientation β and its dispersion as a function of strain. The solid red circles denote labyrinth domain structures with no preferred orientation [see Figs. 3(g) and 3(h)]. The open circle show the cases when there is a preferred DW orientation. The bar shows the dispersion of the angle β. The dashed line is the guide for eyes (in all graphs). (b) The values of β calculated from BLS data using Eq. (3). (c) Average domain width and its dispersion as a function of strain. (d) The iDMI contribution to the DW energy [Eq. (2)] is calculated based on the BLS data. (e) Colored area is the theoretical dependence of the equilibrium orientation of the DW (β) on the iDMI coefficients D_x and D_y. Only the sector $|D_y| < D_x$ is shown. Red circles and black crosses show experimental data obtained by the BLS for the same sample but different applied strain. Red circles correspond to the same strain values (red numbers) as in Fig. 3. The red dashed line is the guide for eyes.

Using the Fourier spectrum one can calculate the mean domain width and DW orientation for different applied strain. We estimate the average width as π/k_{av}, where $k_{av} = \int |\mathbf{k}|F(k_x, k_y)d^2k$ and F is the Fourier spectrum defined in the reciprocal space (k_x, k_y). To estimate the mean DW orientation angle β we first average the Fourier spectrum over the radial direction in the reciprocal space $\tilde{F}(\tilde{\beta}) = \int kF(k, \tilde{\beta})dk$, where the quantities $\tilde{\beta} = \text{atan}(k_y/k_x)$ and $k = |\mathbf{k}|$ are cylindrical coordinates in the reciprocal space. This gives us the angular distribution of the DW orientations $\tilde{F}(\tilde{\beta})$. The angle β is defined by searching for the peaks in the angular dependence $\tilde{F}(\tilde{\beta})$. Dispersion of the DW width and orientation can be also calculated.

The result of the analysis is shown in Figs. 4(a) and 4(c). The circles show the average values of the DW orientation (β) and domain width. The bars show the dispersion of these quantities. In the case of the isotropic labyrinth domain structure (no strain or positive strain), the DW orientation is uniformly distributed over $360°$ ($\tilde{F}(\tilde{\beta}) = \text{const}$). In this case we can not introduce any preferred orientation of DWs and we just put $\beta = 0$ and do not introduce the dispersion. The corresponding points on the graph are shown by the solid red dots. For negative strain the distribution $\tilde{F}(\tilde{\beta})$ shows maxima and we introduce the preferred orientation angle β. It grows up to $40°$ as we increase the compressive strain. The domain width also depends on strain [Fig. 4(c)]. For a compression strain a maximum of the domain width can be observed around $\varepsilon_{xx} = -0.04\%$.

The observed strain-induced domain structure variation can be explained based on the model developed in Ref. [38]. It is shown there that transformation of the isotropic domain

structure into the zigzag one can be induced by varying iDMI. To obtain such a transformation, the iDMI should change from isotropic ($D_x = D_y$) to the strongly anisotropic one with opposite sign along different directions ($D_x = -D_y$). To check the hypothesis we measure iDMI coefficients of the sample as a function of strain.

The measured dependence of the iDMI coefficients D_x and D_y on strain is shown in Fig. 5. For the tensile strain both coefficients increase, but the iDMI stays isotropic ($D_x \approx D_y$). For the compressive strain the strong anisotropy of the iDMI appears and $D_x \neq D_y$. At high enough strain D_y becomes negative while D_x remains positive. Very similar anisotropic
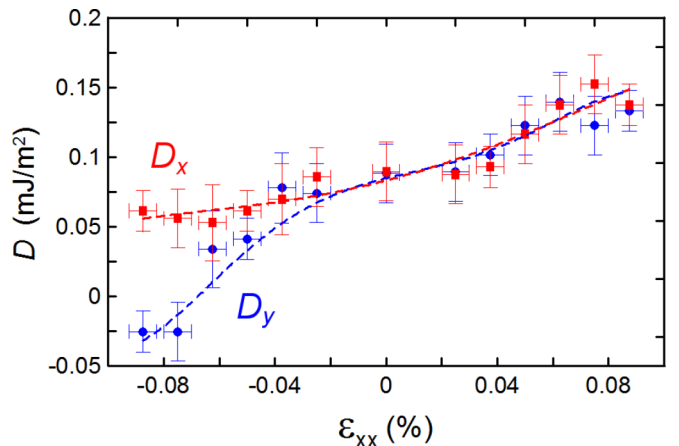
FIG. 5. The DMI constants ($D_{x,y}$) measured along the x (red) and y (blue) directions as a function of applied strain (ε_{xx}). The dashed lines are guides for eyes.

changes of the iDMI under uniaxial deformations were previously observed in Pt/Co/Pt sandwiches [33]. Δf linearly depends on the in-plane component of the wave vector $k_{x,y}$ of the incident beam. The wave vector varies within the range $7 \div 20 \, \mu\text{m}^{-1}$. Thus, relation (1) gives the same values of the iDMI constant for all wave vectors.

Following the approach in Ref. [38] the iDMI contribution to the DW energy is given by

$$W_{\text{dw}}^{\text{DMI}} = -\pi D_+ \cos(2\beta) - \pi D_- + 1/2\kappa\Omega\cos^2(2\beta), \quad (2)$$

where $D_+ = (D_x + D_y)/2$, $D_- = (D_x - D_y)/2$, $\Omega = \mu_0 M_s^2 t = 0.47$ mJ/m^2 ($t = 7.2$ nm is the thickness of the whole multilayer structure) and $\kappa = 0.44$. Minimizing the energy one defines the angle β,

$$\cos(2\beta) = \begin{cases} \dfrac{\pi D_+}{\kappa\Omega}, & \dfrac{\pi D_+}{\kappa\Omega} < 1, \\[2mm] 1, & \dfrac{\pi D_+}{\kappa\Omega} > 1. \end{cases} \quad (3)$$

We calculate β using Eq. (3) and experimental data for D_x and D_y. The result is represented in Fig. 4(b). Obviously, there is a good agreement between the values of β obtained from the analysis of the MFM images and those calculated based on the BLS measurements. Following Ref. [38], we calculated dependence of the orientation angle β on D_x and D_y [Fig. 4(e)]. Different colors in the diagram correspond to different equilibrium values of angles β. The line $D_x = D_y$ corresponds to isotropic iDMI and an isotropic labyrinth domain structure. The violet area ($D_x + D_y > \kappa\Omega/\pi$) corresponds to the domain stripe structure with domains oriented perpendicular to the x axis ($\beta = 0$). In the area $0 < D_x + D_y < \kappa\Omega/\pi$, a gradual increase of β from 0 to $\pi/2$ occurs, which is demonstrated by a smooth color change from blue to red. Note that the energy is the same for four orientations $\pm\beta$ and $\pi \pm \beta$. Because of the degeneracy the zigzag domain structure is formed below in the region $0 < D_x + D_y < \kappa\Omega/\pi$.

We show our experimental data at the diagram in Fig. 4(e). The results of the BLS measurements are shown in the diagram by the crosses indicating error bars for D_x and D_y. Different crosses correspond to different strain values. The points corresponding to the domain structures obtained by the MFM measurements (those shown in Fig. 3) are indicated by thick red circles. Here we also see good agreement between the MFM and BLS results. One can see that the iDMI migrate from isotropic to anisotropic as we apply compressive strain which leads to transformation of the isotropic domain structure to the zigzag one.

The dependence of the domain width provided in Fig. 4(c) has a maximum around $\varepsilon_{xx} = -0.04\%$. It can be understood by analyzing the domain and DW energies. Generally, the domain size is defined by the competition of the DW energy and the magnetostatic energy of domains. The higher the magnetostatic interaction (the higher the magnetization) the smaller the domains. The higher the DW energy the bigger the domains. The magnetization of the film is not affected by strain. Therefore, the magnetostatic energy does not have any peculiarity as a function of strain. The iDMI changes with strain leading to DW energy variation. This should lead to change of the domain width. Based on the BLS data we
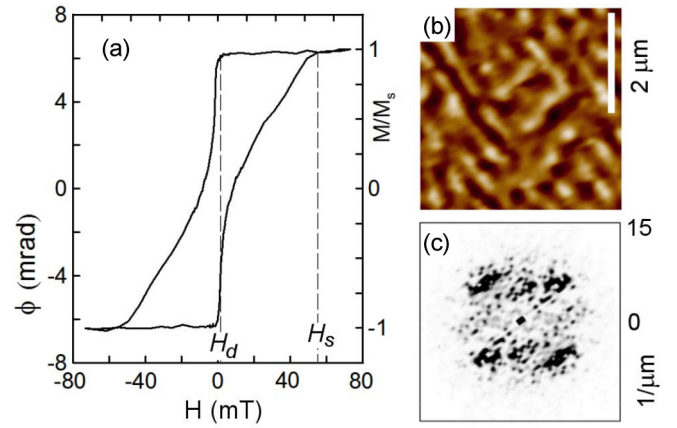
FIG. 6. (a) The MOKE hysteresis loop of the sample with higher $\Delta H_{sd} = H_s - H_d$. (b) The zigzag domains in the compressed sample ($\varepsilon_{xx} = -0.08\%$). (c) The Fourier spectrum of the domain structure.

calculate how the iDMI contribution to DW [Eq. (2)] depends on strain [see Fig. 4(d)]. The iDMI energy has a maximum at compressive strain of about $\varepsilon_{xx} = -0.06\%$. As we have discussed above the maximum of DW energy should correspond to the maximum of domain width. So, the MFM data on the domain width is in agreement with our BLS data and the maximum of the domain width is related to the maximum of the iDMI energy of the DWs.

As we have mentioned earlier, we chose the samples with low ΔH_{sd} to study the strain dependence. Such samples are more sensitive to strain. However, even for samples with higher ΔH_{sd} we can still see strain-induced zigzag domain structure. The results obtained for such a sample are demonstrated in Fig. 6. Figure 6(a) represents the MOKE data showing the hysteresis loop with remnant magnetization of 1. The domain structure in the demagnetized state and its Fourier spectrum for the sample under applied strain ($\varepsilon_{xx} = -0.08\%$) are shown in Figs. 6(b) and 6(c), correspondingly. The zigzag domains (and four spots in the Fourier spectrum) are visible.

Although the strain-induced variation of the iDMI explains the observed changes in the domain structure well, the magnetic anisotropy also changes under mechanical strain. Can the anisotropy variation cause the observed effects? At first, we would like to underline that there is an essential qualitative difference between iDMI variation and anisotropy variation in the case of the uniaxial strain. The influence of the mechanical deformations on the iDMI are described by the phenomenological expression (see symmetry consideration in Ref. [35]).

$$D_x = D_0 + \kappa_1(u_{xx} - u_{yy}) + \kappa_2(u_{xx} + u_{yy}), \quad (4)$$

$$D_y = D_0 - \kappa_1(u_{xx} - u_{yy}) + \kappa_2(u_{xx} + u_{yy}). \quad (5)$$

Here $u_{xx,yy}$ are the main diagonal components of a strain tensor. Taking into account that bending creates a uniaxial strain with $u_{xx} = 0$ and $u_{yy} \neq 0$, the iDMI becomes anisotropic. This means that the iDMI constants along the x and y directions are different. They can be even of different sign along different directions. Such an iDMI anisotropy leads to appearance of four equivalent directions for the magnetization. Finally, this can lead to formation of a zig-zag

domain structure [38]. Due to in-plane anisotropic strain the both out-of-plain magnetic anisotropy and in-plane magnetic anisotropy can change. These changes are described by expression

$$W_{an} \sim \alpha \left(u_{xx} m_x^2 + u_{yy} m_y^2 \right) + \beta u_{zz} m_z^2. \tag{6}$$

Here m_i are the magnetization components, and α and β are some phenomenological constants. Variation of the out-of-plane anisotropy cannot lead to formation of any preferred directions in the sample plane. Therefore, neither stripe nor zig-zag magnetic structures can appear due to the second term. Appearance of the in-plane anisotropy due to anisotropic in-plane strain may induce a preferred magnetization orientation in the sample plane. However, only two equivalent directions may occur, and the zig-zag structure is not allowed due to this symmetry. So, only the anisotropic DMI can be responsible for zig-zag DWs. Therefore, we relate the DMI variation and the DW structure variation.

We also estimate and compare the domain wall energy W_{DW} variation due to the out-of-plane anisotropy variation and DMI variation. The anisotropy-dependent part of the domain wall energy in the thin film can be estimated as $W_{an} \approx 4\sqrt{AK_{eff}}$, where $K_{eff} = K - \Omega/2t$. Taking into account typical value for the exchange stiffness of about 1.5×10^{-11} J/m, we get for the domain wall W_{an} is $\sim 10^{-3}$ J/m^2. The 5% strain-induced variation of the anisotropy constant [33] would lead to 3% variation of the DW energy $\Delta W_{an} \sim 3 \times 10^{-5}$ J/m^2. On the other hand the iDMI-dependent part of the domain wall energy can be estimated as $W_{DMI} \approx \pi D \sim 5 \times 10^{-4}$ J/m^2. This value is twice less but comparable with the W_{an}. This is typical for the Co/Pt multilayers where skyrmions can be observed. The 100% stress-induced iDMI variations lead to an order of magnitude greater DMI contribution ΔW_{DMI} comparing to ΔW_{an}. Finally, the symmetry considerations and the estimate of the domain wall energy variation confirm that the observed effects are associated with strain-induced iDMI variations in the system.

IV. CONCLUSIONS

In summary, we performed MFM and BLS studies of strained Co/Pt multilayered films. We demonstrated that the changes of the iDMI in the system caused by the strain leads to the transformation of the sample's domain structure. The transformation of the isotropic labyrinth domain structure into the stripe and zigzag domains under the strain application is observed. Such a transformation corresponds well to previous theoretical predictions. It happens due to appearance of iDMI anisotropy caused by mechanical deformations. The strain magnitude is not high and can be induced by an electric field in hybrid ferroelectric-ferromagnetic structures. This opens a new way to manipulate magnetic states by an electric field.

[1] F. Bitter, Experiments on the nature of ferromagnetism, Phys. Rev. **41**, 507 (1932).

[2] L. Landau and E. Lifshitz, On the theory of the dispersion of magnetic permeability in ferromagnetic bodies, Phys. Z. Sowjet. **8**, 153 (1935).

[3] D. Atkinson, D. A. Allwood, G. Xiong, M. D. Cooke, C. C. Faulkner, and R. P. Cowburn, Magnetic domain-wall dynamics in a submicrometre ferromagnetic structure, Nat. Mater. **2**, 85 (2003).

[4] A. Yamaguchi, T. Ono, S. Nasu, K. Miyake, K. Mibu, and T. Shinjo, Real-Space Observation of Current-Driven Domain Wall Motion in Submicron Magnetic Wires, Phys. Rev. Lett. **92**, 077205 (2004).

[5] M. Hayashi, L. Thomas, R. Moriya, C. Rettner, and S. S. Parkin, Current-controlled magnetic domain-wall nanowire shift register, Science **320**, 209 (2008).

[6] Z. Luo, A. Hrabec, T. P. Dao, G. Sala, S. Finizio, J. Feng, S. Mayr, J. Raabe, P. Gambardella, and L. J. Heyderman, Current-driven magnetic domain-wall logic, Nature (London) **579**, 214 (2020).

[7] B. Garbin, J. Fatome, G.-L. Oppo, M. Erkintalo, S. G. Murdoch, and S. Coen, Dissipative Polarization Domain Walls in a Passive Coherently Driven Kerr Resonator, Phys. Rev. Lett. **126**, 023904 (2021).

[8] V. Jeudy, R. Diaz Pardo, W. Savero Torres, S. Bustingorry, and A. B. Kolton, Pinning of domain walls in thin ferromagnetic films, Phys. Rev. B **98**, 054406 (2018).

[9] L. Caretta, M. Mann, F. Büttner, K. Ueda, B. Pfau, C. M. Günther, P. Hessing, A. Churikova, C. Klose, M. Schneider, D. Engel, C. Marcus, D. Bono, K. Bagschik, S. Eisebitt, and G. S. D. Beach, Fast current-driven domain walls and small skyrmions in a compensated ferrimagnet, Nat. Nanotech. **13**, 1154 (2018).

[10] G. Tatara and H. Kohno, Theory of Current-Driven Domain Wall Motion: Spin Transfer versus Momentum Transfer, Phys. Rev. Lett. **92**, 086601 (2004).

[11] O. A. Tretiakov, D. Clarke, G.-W. Chern, Y. B. Bazaliy, and O. Tchernyshyov, Dynamics of Domain Walls in Magnetic Nanostrips, Phys. Rev. Lett. **100**, 127204 (2008).

[12] A. V. Khvalkovskiy, V. Cros, D. Apalkov, V. Nikitin, M. Krounbi, K. A. Zvezdin, A. Anane, J. Grollier, and A. Fert, Matching domain-wall configuration and spin-orbit torques for efficient domain-wall motion, Phys. Rev. B **87**, 020402(R) (2013).

[13] D. Wang and Y. Zhou, Algebraic decay of the nonadiabaticity arising through chiral spin transfer torque in magnetic domain walls with Rashba spin-orbit interaction, Phys. Rev. B **101**, 184428 (2020).

[14] H. Kazemi, S. Eggert, and N. Sedlmayr, Local spin transfer torque and magnetoresistance in domain walls with variable width, Phys. Rev. B **102**, 064404 (2020).

[15] S. S. P. Parkin, M. Hayashi, and L. Thomas, Magnetic domain-wall racetrack memory, Science **320**, 190 (2008).

[16] A. Hoffmann and S. D. Bader, Opportunities at the Frontiers of Spintronics, Phys. Rev. Appl. **4**, 047001 (2015).

[17] D. A. Allwood, G. Xiong, C. C. Faulkner, D. Atkinson, D. Petit, and R. P. Cowburn, Magnetic domain-wall logic, Science **309**, 1688 (2005).

[18] A. Schellekens, A. van den Brink, J. Franken, H. J. M. Swagten, and B. Koopmans, Electric-field control of domain wall motion in perpendicularly magnetized materials, Nat. Commun. **3**, 847 (2012).

[19] N. Lei, T. Devolder, G. Agnus, P. Aubert, L. Daniel, J.-V. Kim, W. Zhao, T. Trypiniotis, R. P. Cowburn, C. Chappert, D. Ravelosona, and P. Lecoeur, Strain-controlled magnetic domain wall propagation in hybrid piezoelectric/ferromagnetic structures, Nat. Commun. **4**, 1378 (2013).

[20] J. Dean, M. T. Bryan, T. Schrefl, and D. A. Allwood, Stress-based control of magnetic nanowire domain walls in artificial multiferroic systems, J. Appl. Phys. **109**, 023915 (2011).

[21] C.-J. Hsu, J. L. Hockel, and G. P. Carman, Magnetoelectric manipulation of domain wall configuration in thin film Ni/[Pb(Mn$_{1/3}$Nb$_{2/3}$)O$_3$]$_{0.68}$-[PbTiO$_3$]$_{0.32}$ (001) heterostructure, Appl. Phys. Lett. **100**, 092902 (2012).

[22] H. Ohno, D. Chiba, F. Matsukura, T. Omiya, E. Abe, T. Dietl, Y. Ohno, and K. Ohtani, Electric-field control of ferromagnetism, Nature (London) **408**, 944 (2000).

[23] M. Endo, S. Kanai, S. Ikeda, F. Matsukura, and H. Ohno, Electric-field effects on thickness dependent magnetic anisotropy of sputtered structures, Appl. Phys. Lett. **96**, 212503 (2010).

[24] M. V. Sapozhnikov, Skyrmion lattice in a magnetic film with spatially modulated material parameters, J. Magn. Magn. Mater. **396**, 338 (2015).

[25] M. V. Sapozhnikov, N. S. Gusev, S. A. Gusev, D. A. Tatarskiy, Yu. V. Petrov, A. G. Temiryazev, and A. A. Fraerman, Direct observation of topological Hall effect in Co/Pt nanostructured films, Phys. Rev. B **103**, 054429 (2021).

[26] A. Bogdanov and A. Hubert, Thermodynamically stable magnetic vortex states in magnetic crystals, J. Magn. Magn. Mater. **138**, 255 (1994).

[27] P. Ferriani, K. von Bergmann, E. Y. Vedmedenko, S. Heinze, M. Bode, M. Heide, G. Bihlmayer, S. Blugel, and R. Wiesendanger, Atomic Scale Spin Spiral with a Unique Rotational Sense: Mn Monolyer on W(001), Phys. Rev. Lett. **101**, 027201 (2008).

[28] M. Heide, G. Bihlmayer, and S. Blugel, Dzyaloshinskii-Moriya interaction accounting for the orientation of magnetic domains in ultrathin films: Fe/W (110), Phys. Rev. B **78**, 140403(R) (2008).

[29] A. Fert, Magnetic and transport properties of metallic multilayers, Mater. Sci. Forum **59**, 439 (1990).

[30] G. Chen, J. Zhu, A. Quesada, J. Li, A. T. N'Diaye, Y. Huo, T. P. Ma, Y. Chen, H. Y. Kwon, C. Won, Z. Q. Qiu, A. K. Schmid, and Y. Z. Wu, Novel Chiral Magnetic Domain Wall Structure in Fe/Ni/Cu(001) Films, Phys. Rev. Lett. **110**, 177204 (2013).

[31] M. J. Benitez, A. Hrabec, A. P. Mihai, T. A. Moore, G. Burnell, D. McGrouther, C. H. Marrows, and S. McVitie, Magnetic microscopy and topological stability of homochiral Néel domain walls in a Pt/Co/AlO$_x$ trilayer, Nat. Commun. **6**, 8957 (2015).

[32] T. N. G. Meier, M. Kronseder, and C. H. Back, Domain-width model for perpendicularly magnetized systems with Dzyaloshinskii-Moriya interaction, Phys. Rev. B **96**, 144408 (2017).

[33] N. S. Gusev, A. V. Sadovnikov, S. A. Nikitov, M. V. Sapozhnikov, and O. G. Udalov, Manipulation of the Dzyaloshinskii-Moriya Interaction in Co/Pt Multilayers with Strain, Phys. Rev. Lett. **124**, 157202 (2020).

[34] O. G. Udalov and I. S. Beloborodov, Strain-dependent Dzyaloshinskii-Moriya interaction in a ferromagnet/heavy-metal bilayer, Phys. Rev. B **102**, 134422 (2020).

[35] O. G. Udalov, I. S. Beloborodov, and M. V. Sapozhnikov, Magnetic skyrmions and bimerons in films with anisotropic interfacial Dzyaloshinskii-Moriya interaction, Phys. Rev. B **103**, 174416 (2021).

[36] Y. Ba, S. Zhuang, Y. Zhang, Y. Wang, Y. Gao, H. Zhou, M. Chen, W. Sun, Q. Liu, G. Chai, J. Ma, Y. Zhang, H. Tian, H. Du, W. Jiang, C. Nan, J.-M. Hu, and Y. Zhao, Electric-field control of skyrmions in multiferroic heterostructure via magnetoelectric coupling, Nat. Commun. **12**, 322 (2021).

[37] J. Cui, J. L. Hockel, P. K. Nordeen, D. M. Pisani, C.-y. Liang, G. P. Carman, and C. S. Lynch, A method to control magnetism in individual strain-mediated magnetoelectric islands, Appl. Phys. Lett. **103**, 232905 (2013).

[38] O. G. Udalov and M. V. Sapozhnikov, Orientation and internal structure of domain walls in ferromagnetic films with anisotropic Dzyaloshinskii-Moriya interaction, J. Magn. Magn. Mater. **519**, 167464 (2021).

[39] L. Landau and E. Lifshitz, *Electrodynamics of Continuous Media* (Pergamon Press, Oxford, 1984).

[40] L. Angeloni, D. Passeri, M. Reggente, D. Mantovani, and M. Rossi, Removal of electrostatic artifacts in magnetic force microscopy by controlled magnetization of the tip: Application to superparamagnetic nanoparticles, Sci. Rep. **6**, 26293 (2016).

[41] K. Di, V. L. Zhang, H. S. Lim, S. C. Ng, M. H. Kuok, J. Yu, J. Yoon, X. Qiu, and H. Yang, Direct Observation of the Dzyaloshinskii-Moriya Interaction in a Pt/Co/Ni Film, Phys. Rev. Lett. **114**, 047201 (2015).

[42] E. S. Demidov, N. S. Gusev, L. I. Budarin, E. A. Karashtin, V. L. Mironov, and A. A. Fraerman, Interlayer interaction in multilayer [Co/Pt]$_n$/Pt/Co structures, J. Appl. Phys. **120**, 173901 (2016).

[43] M. V. Sapozhnikov, S. N. Vdovichev, O. L. Ermolaeva, N. S. Gusev, A. A. Fraerman, S. A. Gusev, and Yu. V. Petrov, Artificial dense lattice of magnetic bubbles, Appl. Phys. Lett. **109**, 042406 (2016).

[44] S. Woo, K. Litzius, B. Krüger, M.-Y. Im, L. Caretta, K. Richter, M. Mann, A. Krone, R. M. Reeve, M. Weigand, P. Agrawal, I. Lemesh, M.-A. Mawass, P. Fischer, M. Klaui, and G. S. D. Beach, Observation of room-temperature magnetic skyrmions and their current-driven dynamics in ultrathin metallic ferromagnets, Nat. Mater. **13**, 501 (2016).

[45] M. V. Sapozhnikov, Y. V. Petrov, N. S. Gusev, A. G. Temiryazev, O. L. Ermolaeva, V. L. Mironov, and O. G. Udalov, Artificial dense lattices of magnetic skyrmions, Materials **13**, 99 (2020).

[46] B. Hillebrands, Spin-wave calculations for multilayered structures, Phys. Rev. B **41**, 530 (1990).

[47] O. Gladii, M. Haidar, Y. Henry, M. Kostylev, and M. Bailleul, Frequency nonreciprocity of surface spin wave in permalloy thin films, Phys. Rev. B **93**, 054430 (2016).

[48] M. V. Sapozhnikov, O. V. Ermolaeva, E. V. Skorokhodov, N. S. Gusev, and M. N. Drozdov, Magnetic skyrmions inthickness-modulated films, JETP Lett. **107**, 364 (2018).